AIAA 80-1107R

Calculation of High-Speed Inlet Flows Using the Navier-Stokes Equations

Doyle D. Knight*
Rutgers University, New Brunswick, N.J.

A numerical code has been developed to calculate the flowfield in two-dimensional high-speed inlets using the Navier-Stokes equations. Arbitrary inlet geometries may be treated, with variable bleed on the ramp and cowl surfaces. Turbulence is incorporated through an algebraic turbulent eddy viscosity. The code has been applied to the calculation of the flow in a simulated high-speed inlet operating at a Mach number of 2.5 and Reynolds number of 1.4×10^7 based on inlet length. Two different bleed schedules were considered, which differed principally in the extent of bleed in the vicinity of the shock-turbulent boundary interactions on the ramp surface. The computed results are compared with detailed measurements of the ramp and cowl static pressures, and boundary-layer pitot profiles. The agreement with the experimental data is generally good, although the experimental data display evidence of three dimensionality over a portion of the inlet flowfield.

Nomenclature

$\dot{m}$ = bleed mass flux $=\rho_w v_w$ ($\dot{m}<0$ for bleed)
p = static pressure
p_p = pitot pressure
p_t = total pressure
u_* = friction velocity $=\sqrt{\tau_w/\rho_w}$
v_w = bleed velocity at wall
x,y,z = Cartesian coordinates
y' = distance normal to wall
y'_m = height of computational sublayer
$\Delta\zeta,\Delta\eta$ = mesh spacing in ζ and η directions
δ_0 = reference boundary-layer thickness for relaxation model
δ = boundary-layer thickness
ϵ = turbulent eddy viscosity
ζ,η = transformed coordinates
λ = relaxation length
ν = kinematic viscosity
ρ = density
τ = shear stress

Subscripts

∞ = evaluated upstream of body
w = evaluated at wall

Introduction

THE accurate prediction of the performance of high-speed aircraft inlets poses a serious challenge to the aircraft designer. In many cases the structure of the inlet internal flow is complex. For example, in a mixed-compression supersonic inlet operating at critical conditions, the internal flow structure consists of a pattern of oblique shock waves and (possibly) expansion fans, terminated by an approximately normal shock near the inlet throat. The interaction of the shock waves with the cowl and ramp boundary layers can seriously affect the inlet performance if, for example, boundary-layer separation occurs. Flow separation in the subsonic diffuser results in decreased total pressure recovery and increased total pressure distortion at the compressor face, while separation within the supersonic portion of the inlet can cause flow instability and inlet unstart. The conventional technique of preventing flow separation is the use of distributed bleed on the inlet internal surfaces. However, the use of bleed causes a drag penalty, and thus it is desirable to utilize the minimum bleed necessary to provide the required inlet performance.

The traditional approach to theoretical inlet design and analysis is based on the separate or coupled treatment of the inviscid and viscous portions of the inlet flow. The inviscid flow is calculated by either the method of characteristics[1,2] or inviscid finite-difference shock-capturing techniques.[3] The effect of the boundary-layer displacement thickness is either ignored[2-4] or incorporated as a correction.[5] The interaction of the shock waves with the boundary layers is treated by semiempirical models.[5]

A major advantage of the traditional approach, as compared to methods employing the full Navier-Stokes equations discussed subsequently, is computational efficiency. The typical computer time required for an inviscid shock-capturing finite-difference calculation of an axisymmetric inlet flowfield[3] is approximately 15 s on a CDC 7600 (approximately 75 s on an IBM 370/168). Since the cost per flow calculation is very low, a wide range of inlet operating conditions can be considered for the same amount of computer time required for a single Navier-Stokes calculation.

There are several major disadvantages, however, associated with the traditional approach. First, the use of semiempirical models of shock-boundary layer interaction (SBLI) oftentimes yields incorrect predictions of the reflected shock wave structure and consequently unreliable performance predictions.[5,6] Second, the conventional method of characteristics and inviscid finite-difference shock-capturing techniques are limited to supersonic flow. Thus, the development of any subsonic region terminates the computation, which in practice may occur upstream of the inlet throat.[5] Third, these methods are incapable of handling flow separation due to inadequate treatment of strong viscous-inviscid interactions. The effects of flow separation on inlet performance at high angles of attack is a major concern in aircraft design.[7]

The disadvantages of the traditional approach can be overcome by utilizing the Navier-Stokes equations. The capability of accurate calculation of high-speed flows with strong viscous-inviscid interaction has been clearly demonstrated in recent years. A brief sampling of cases includes the interaction of a shock wave with the boundary layer on a flat plate,[8,9] supersonic flow in a compression corner,[10] transonic airfoil flows,[11] hypersonic flow over indented nosetips,[12] the

Received May 23, 1980; presented as Paper 80-1107 at the AIAA/SAE/ASME 16th Joint Propulsion Conference, Hartford, Conn., June 30-July 2, 1980; revision received Feb. 18, 1981.

*Associate Professor, Department of Mechanical and Aerospace Engineering. Member AIAA.

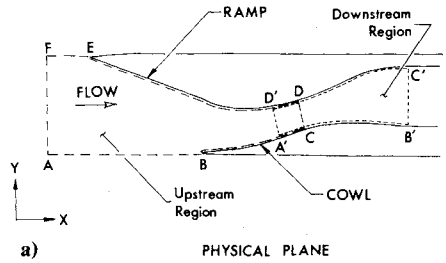

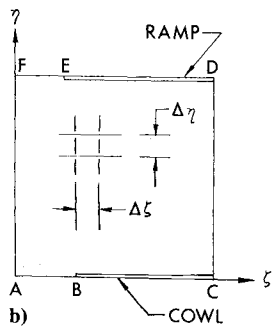

Fig. 1 a) Details of inlet geometry. b) Details of upstream transformed plane.

oscillatory flowfield associated with supersonic flow past a spike-tipped body,[13] and two-dimensional high-speed inlets.[14,15]

The purpose of this investigation is to apply an improved Navier-Stokes computer code[15] to the calculation of the flowfield in a high speed inlet. Attention is focused on the effect of various boundary-layer bleed schedules on the inlet flow structure for the specific case of a simulated high-speed inlet at a Mach number of 2.5 and Reynolds number of 1.4×10^7 based on inlet length.

Method of Solution

A complete description of the Navier-Stokes code is available in Refs. 15 and 16, and thus is only summarized here. A set of curvilinear coordinates $\zeta(x,y)$ and $\eta(x,y)$, obtained from two Poisson equations,[15-17] are introduced to map a general curvilinear computational region in the physical (x,y) plane (e.g., region ABCDEF or A'B'C'D' in Fig. 1a) into unit square in the transformed (ζ,η) plane. The mesh distribution in the transformed plane is uniform, while its image in the physical plane is a highly nonuniform grid capable of resolving the significant features of the flowfield including the ramp and cowl boundary layers.

The numerical code employs the full mean compressible Navier-Stokes equations in mass-averaged variables[18] for two-dimensional turbulent flow. Turbulence is represented by the two-layer algebraic equilibrium eddy viscosity model of Cebeci and Smith,[19] together with the transition model of Dhawan and Narasimha.[20,21] The turbulent eddy viscosity relaxation model of Shang and Hankey[10] is incorporated for use in the vicinity of strong shock-wave turbulent boundary-layer interaction. The relaxation model is not employed, however, in the presence of boundary-layer bleed due to a lack of previous experience in such cases. The turbulent eddy viscosity $\epsilon(s,n)$ at a distance s from the leading edge and distance n from the surface is given by

$$\epsilon(s,n)=\epsilon_{eq}(s_0,n)+[\epsilon_{eq}(s,n)-\epsilon_{eq}(s_0,n)]\times[1-\exp(-(s-s_0)/\lambda)] \quad (1)$$

where s_0 is a location approximately seven boundary-layer thicknesses upstream of the intersection of the shockwave and the wall, ϵ_{eq} the equilibrium eddy viscosity of Cebeci and Smith, and λ typically[22] 10-20 times the boundary-layer thickness δ_0 at s_0.

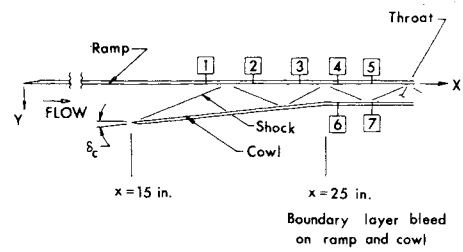

Fig. 2 Geometry of high-speed inlet.

For reasons of computational economy, the inlet flowfield is subdivided into a number of overlapping computational regions as illustrated in Fig. 1a. Beginning with the upstream region ABCDEF, the flow in each region is converged to steady state. The values of the flow variables at the restart station A'D' are then employed as the upstream profile for the second computational region A'B'C'D'. Details of the boundary conditions are given in Refs. 15 and 16.

The numerical algorithm is MacCormack's explicit finite-difference method,[8,9] which is an alternating-direction technique of second-order accuracy. The procedure consists of integrating the governing equations in time from an assumed (and, in practice, rather arbitrary) initial condition until a steady-state flowfield is achieved. Several traditional techniques have been incorporated to improve computational efficiency, including time splitting of the finite-difference operators and splitting of the mesh into several regions in the cross-streamwise direction.[15] In addition, a separate and efficient treatment of the region containing the viscous sublayer and transition portion of the turbulent boundary layer [denoted the computational sublayer (CSL)] is employed.[15] This region is taken to be $0\le y'\le 60\nu_w/u_*$, where y' is the distance normal to the wall. For these results, the governing equations in the CSL were solved as a nonlinear two-point boundary value problem using the second-order accurate box scheme[23] (centered Euler scheme) and Newton iteration.

The numerical code has been tested rigorously for a variety of flows including a turbulent boundary layer on a flat plate, the interaction of a shock wave with a turbulent boundary layer (in which flow separation was observed), and three different configurations of a simulated high-speed inlet. In all cases, comparison of the computed results with experimental data and previous numerical calculations by other individuals was quite favorable.[15,16] The numerical code displays a high degree of "robustness," in that for all cases considered to date there has been no evidence of numerical instability.

High-Speed Inlet Calculations

Description

The configuration is the simulated rectangular high-speed inlet investigated by Carter and Spong[24] (see Fig. 2). A converging supersonic diffuser is formed by two nonparallel plates, followed by a constant-height "throat" with the upper and lower surfaces analogous to the ramp and cowl, respectively, of a high-speed inlet. A single oblique shock-wave train, formed by the deflection δ_c of the cowl surface, interacts with the turbulent boundary layers on the ramp and cowl. Boundary-layer bleed is provided in three separate bleed zones each on both the ramp and cowl surfaces.

The experimental data consist of ramp and cowl static pressures and boundary-layer pitot profiles. The static taps were located on the duct centerline, except for an additional spanwise pair on the ramp only at $x=43.2$, 57.8, and 66.0 cm. There were five pairs of boundary-layer pitot rakes on the ramp (stations 1-5 in Fig. 2), located off the duct centerline. The rakes were positioned upstream and downstream of the

Table 1 Ramp boundary-layer bleed schedule

Case	Bleed zone	Region, cm	$\dot{m}/\rho_\infty U_\infty$
1	1	$41.9 \le x \le 49.0$	−0.0106
(Complete bleed)	2a	$49.0 \le x \le 58.8$	−0.0154
	2b	$58.8 \le x \le 62.8$	−0.0046
	3	$62.8 \le x \le 67.3$	−0.0214
2	1	No bleed	
(Partial bleed)	2	$58.8 \le x \le 61.6$	−0.0286
	3	$61.6 \le x \le 67.3$	−0.0219

Table 2 Cowl boundary-layer bleed schedule

Case	Bleed zone	Region, cm	$\dot{m}/\rho_\infty U_\infty$
1	1	$49.4 \le x \le 58.4$	−0.0032
	2	$58.4 \le x \le 63.2$	−0.0134
	3	$65.4 \le x \le 67.3$	−0.0158
2	1	$49.4 \le x \le 57.8$	−0.0041
	2	$57.8 \le x \le 63.2$	−0.0127
	3	$65.4 \le x \le 67.3$	−0.0219

Table 3 Computational regions

Case	Region	Extent, cm	Δx, cm
Upstream	1	$-2.2 \le x \le 22.5$	0.64
	2	$17.5 \le x \le 42.2$	0.64
1	1	$36.7 \le x \le 49.0$	0.318
	2	$46.2 \le x \le 58.6$	0.318
	3	$55.7 \le x \le 68.1$	0.318
	4	$65.5 \le x \le 74.1$	0.318
2	1	$36.7 \le x \le 49.0$	0.318
	2	$44.3 \le x \le 56.7$	0.318
	3	$53.5 \le x \le 65.9$	0.318
	4	$64.3 \le x \le 74.1$	0.318

shock-boundary layer interactions on the ramp. There were two single rakes on the cowl (stations 6 and 7 in Fig. 2) located off the duct centerline.

The present study focuses on the effect of various ramp and cowl boundary-layer bleed schedules on the inlet internal flow structure. Two cases were considered that differed only in their bleed schedules. The cowl angle $\delta_c = 8.025$ deg, and the throat height is 3.56 cm. The freestream Mach number $M_\infty = 2.50$, and the freestream stagnation pressure p_{t_∞} and temperature T_{t_∞} are 206.6 kPa and 323 K, respectively, yielding a Reynolds number of 1.4×10^7 based on the total model length of 78.7 cm. The bleed schedules are indicated in Tables 1 and 2. In case 1 ("complete bleed"), bleed is provided along a large portion of the ramp surface which includes the first and second SBLI on the ramp. In case 2 ("partial bleed"), bleed is provided on the ramp over an area covering only the second SBLI on the ramp. The regions of bleed on the cowl are nearly identical for both cases, and cover the first and second SBLIs on the cowl.

Details of Computation

The calculation was performed in two phases.[15] In the first phase, the region upstream of the inlet entrance (i.e., the boundary layer on the ramp) was calculated using two overlapping regions. In the second phase, the flow data at $x = 36.7$ cm were employed as the upstream profiles for calculation of the inlet internal flow. A total of four overlapping computational regions were utilized in calculating the internal flowfield for each case. The areas of overlap were specifically chosen to insure that the requirements imposed by the overlapping technique were met in all instances as discussed in Ref. 15. The extent of the computational regions is indicated in Table 3.

Table 4 Mesh resolution

Case	IL	JL	JSL0	JSL1	Max Δy_{SL}^+	Max $y_m'^+$
Upstream	71	35	20	–	2.2	41.9
1	119	48	20	20	2.7	58.4
2	119	48	20	20	2.9	54.8

Table 5 Computer times

Case	Region	t/t_c	N_{coarse}	Computer time on IBM 370/168, h
Upstream	1	1.7	270	0.32
	2	1.6	275	0.38
			Total	0.70
1	1	3.2	112	0.74
	2	2.8	182	1.20
	3	2.8	236	2.32
	4	2.9	196	1.04
			Total	5.30
2	1	2.8	106	0.54
	2	4.9	255	1.72
	3	3.8	312	3.58
	4	3.0	240	1.54
			Total	7.38

Accurate numerical simulation of high-speed flows exhibiting strong viscous-inviscid interactions requires careful treatment of the computational mesh. Unfortunately, precise criteria do not exist except for a truncation error analysis using successively refined grids which is impractical. However, approximate criteria have been developed based on extensive numerical experience (a list of references is provided in Ref. 15). These may be divided into two major areas, namely 1) resolution of the flowfield in the cross-streamwise direction, and 2) resolution of flowfield in the streamwise direction. The resolution of the flow in the cross-streamwise direction is critically important within the boundary layers. The criteria are 1) the viscous sublayer mesh spacing Δy_{SL} satisfies $\Delta y_{SL}^+ \lesssim 5$ where $\Delta y_{SL}^+ = \Delta y_{SL}\, u_* N/\nu_w$, where N is a modification to the Van Driest damping factor[15]; 2) the height y_m' of the computational sublayer satisfies $y_m' \lesssim 60\nu_w/u_*$; and 3) the total number of mesh points within each boundary layer should be at least 15. The second criterion is applicable to the present code only.[15] The details of the mesh distribution are indicated in Table 4, where IL is the total number of points in the ζ direction (overlapped points for each case are counted only once), JL is the number of ordinary mesh points in the η direction,[15] and JSL0 and JSL1 are the number of mesh points in the computational sublayer on the ramp and cowl, respectively. The term max Δy_{SL}^+ is the maximum value of Δy_{SL}^+ taken over all stations on the ramp and cowl and max$y_m'^+$ is the corresponding maximum of $y_m' u_*/\nu_w$. The results clearly indicate satisfaction of criteria 1 and 2. The typical total number of mesh points in either the ramp or cowl boundary layer is 35-40, thus satisfying criteria 3.

The resolution of the flow in the streamwise direction is critically important within regions of shock-boundary layer interaction. A commonly accepted criterion is based on the ratio $\Delta x/\delta$, where Δx is the streamwise mesh spacing and δ the boundary-layer thickness immediately upstream of the interaction. Acceptable values of $\Delta x/\delta$ range from 0.25 to 1.17, depending on the particular flow problem, with $\Delta x/\delta$ generally less than 0.5 for flows with separation.[15] In the present study, $\Delta x/\delta$ is equal to 0.42 for the first SBLI on the ramp in both cases. For the second and third ramp SBLI the values are 0.83 and 1.0, respectively, for case 1, and 0.48 and

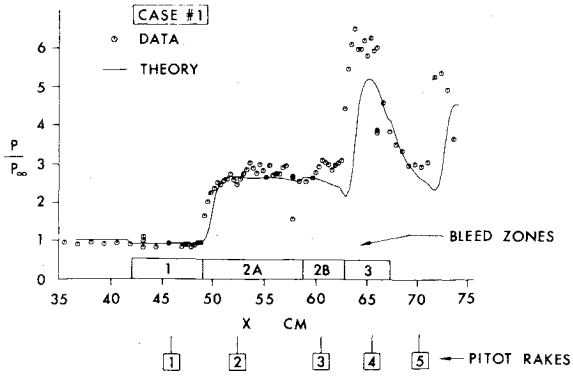

Fig. 3 Static pressure on ramp for case 1.

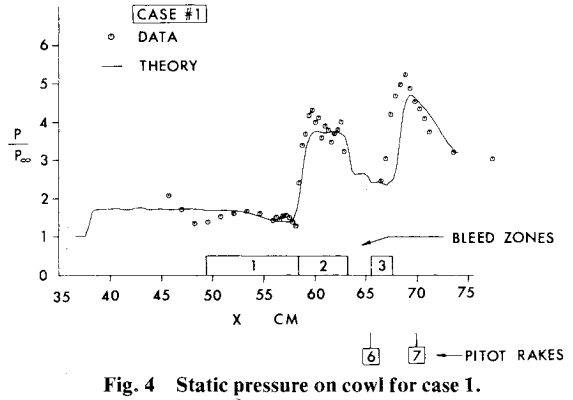

Fig. 4 Static pressure on cowl for case 1.

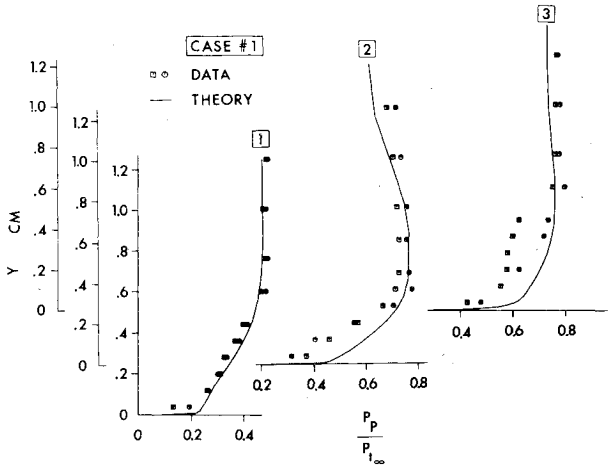

Fig. 5 Pitot pressure profiles on ramp at stations 1-3 for case 1.

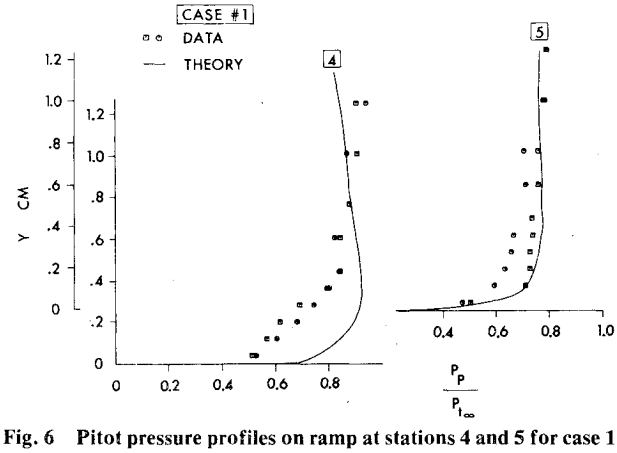

Fig. 6 Pitot pressure profiles on ramp at stations 4 and 5 for case 1.

0.45 for case 2, respectively. For the cowl SBLIs, the values of $\Delta x/\delta$ were less than 1.2 for both cases. Flow separation was only observed for case 2 at the first ramp SBLI, and therefore the resolution afforded by streamwise mesh spacing is considered sufficient.

The criterion employed for determining convergence of the flowfield to steady state is based on the total physical time of integration of the flow.[15] Experience indicates that convergence in a given computational region is achieved for unseparated flows after a physical time of $2t_c$-$3t_c$, where t_c is the time required for a fluid particle to traverse the length of the region in the inviscid portion of the flow.[14,15] For separated flows (e.g., in region 2 of case 2), approximately $5t_c$-$6t_c$ is required. All computations were performed on an IBM 370/168 computer using single-precision (32 bit word) arithmetic, except for the matrix inversions associated with the computational sublayer algorithm which employed double precision. Previous results have clearly demonstrated that single-precision arithmetic is entirely adequate for this code.[15] The numerical code was compiled using the Fortran H (Opt = 2) compiler. The computer times are listed in Table 5, along with the average total number of time steps N_{coarse} in the coarse mesh region (i.e., region 3 of Fig. 1c in Ref. 15). The expected run times on the CYBER 175 used in previous investigations[15,16] would be approximately half that of the IBM 370/168.

Results for Case 1 (Complete Bleed)

The computed and measured ramp static pressure is presented in Fig. 3. The numbered bleed regions are also shown, together with the locations of the five ramp pitot rake stations. The agreement in the vicinity of the first SBLI at $x = 50$ cm is very good. The computed ramp pressure rise associated with the second SBLI near $x = 65$ cm is shifted downstream slightly compared to the experimental data, with a computed peak pressure approximately 15% too low. This slight downstream displacement, evident also at the third SBLI near $x = 72$ cm, is an apparent result of the shock-capturing nature of the numerical algorithm and has been observed in previous studies.[15] The computed and measured ramp pressures are in close agreement in the expansion region between $x = 66$ and 70 cm, which is associated with the impingement of the expansion fan originating at the cowl hinge line.

In Fig. 4, the computed and measured cowl static pressure is displayed. The computed results indicate an abrupt pressure rise at $x = 38$ cm associated with the cowl shock. The agreement is very good in the vicinity of the first cowl SBLI at $x = 59$ cm. The computed cowl pressure again displays the characteristic slight downstream shift in the neighborhood of the second cowl SBLI at $x = 67$ cm, with the peak pressure within 10% of the data. The computed and measured cowl pressure in the expansion region from $x = 70$ to 75 cm are in reasonable agreement.

The boundary-layer development on the ramp is shown in Figs. 5 and 6. The experimental data from the two pitot pressure rakes at each station is indicated by the circle and square symbols. The computed pitot pressure profile at station 1, located upstream of the first SBLI on the ramp, is in excellent agreement with the experimental data. The modified Van Driest damping factor developed by Cebeci[25] for turbulent boundary layers with mass transfer evidently has been examined only for a limited range of values of the dimensionless wall normal velocity $v_w^+ = v_w/u_*$, namely the range $-0.05 \le v_w^+ \le 1.0$. The value of v_w^+ at station 1 is -0.179, indicating a greater range of validity of the turbulence model in equilibrium turbulent flows. The computed profile at station 2, positioned downstream of the first ramp SBLI, is in close agreement with the measured values except for $y < 0.20$ cm where calculated profile is somewhat fuller. The value of v_w^+ at station 2 is -0.137, which is apparently within the

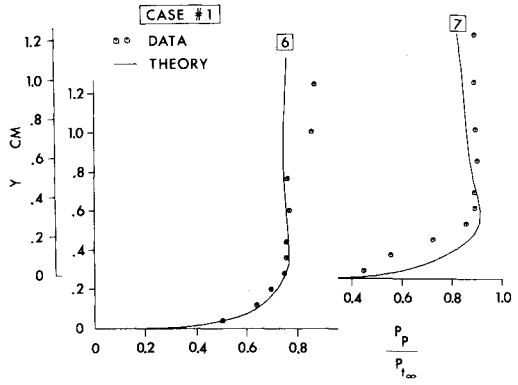

Fig. 7 Pitot pressure profiles on cowl at stations 6 and 7 for case 1.

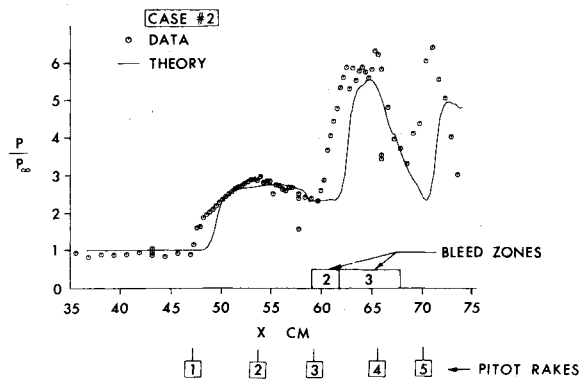

Fig. 8 Static pressure on ramp for case 2.

range of proven validity of the equilibrium turbulence model as indicated earlier. Nevertheless, station 2 is immediately downstream of the first ramp SBLI, and experience indicates that equilibrium turbulence models such as that of Cebeci are of limited accuracy within regions of strong viscous-inviscid interaction.[10,26] In particular, the computed results indicated that the eddy viscosity in the inner portion of the boundary layer was strongly controlled by the boundary-layer bleed and affected to a lesser extent by the shock-boundary layer interaction. This suggests that the problem of turbulent shock-boundary layer interaction in the presence of strong bleed displays additional features, such as the combined effects of rapid pressure rise and possible laminarization of the flow near the wall due to strong suction. The computed profile at station 3, located upstream of the second SBLI on the ramp, is in general agreement with the measured values, although displaying the characteristic fuller profile near the wall seen previously. The value of v_w^+ at station 3 is -0.063.

In Fig. 6, the pitot pressure profiles are presented at ramp stations 4 and 5 on the ramp, which are downstream of the second ramp SBLI and upstream of the third ramp SBLI, respectively. At station 4, there is a pronounced discrepancy between the computed and measured pitot pressure for $y<0.50$ cm. A number of factors may account for this disagreement, including limitations of the turbulence model as previously discussed, and three-dimensional effects in the vicinity of the second ramp SBLI as evidenced by the spanwise ramp pressure variation at $x=66$ cm. In particular, the three spanwise pressures are 46.1, 47.0, and 72.8 kPa. In earlier studies,[15] a similar three-dimensional character was observed at the second ramp SBLI. The computed pitot profile at station 5 is in reasonable agreement with the experimental data.

The cowl boundary-layer development is evident in Fig. 7, where results are displayed for stations 6 and 7 located upstream and downstream of the second cowl SBLI. The computed profile at station 6 displays excellent agreement with experiment, while the profile at station 7 is somewhat fuller than the observations.

Results for Case 2 (Partial Bleed)

The computed and measured ramp static pressure is indicated in Fig. 8. The computed pressure rise associated with the first ramp SBLI begins at $x=48.3$ cm and ends at approximately $x=52$ cm. The calculations display a region of flow separation (i.e., negative skin friction) extending from $x=49.2$ to 50.6 cm. The experimental pressure rise begins, however, at $x=47.0$ cm and ends at approximately 53.3 cm. Flow separation was also evidently present in the experiment[24] according to the empirical criterion of Kuehn.[27]

The discrepancy in the sizes of the computed and experimental interaction regions is perhaps somewhat surprising, based on previous success in computing shock-turbulent boundary-layer interaction on a flat plate.[15,22] In seeking an explanation of this difference, several points must be considered, namely, 1) the accuracy of the finite-difference calculation (i.e., truncation error effects), 2) the sensitivity of the computed solution to the parameters in the turbulence model (specifically, the relaxation length λ), and 3) the possibility of significant three-dimensional flow in the vicinity of the separation region. In examining the first point, the data in Table 4 indicate that the mesh resolution in the cross-streamwise direction is more than sufficient based on experience.[15] In order to judge the effect of the streamwise mesh spacing, region 2 of case 2 containing the first ramp SBLI was recomputed with $\Delta x=0.3\ \delta_0$, compared to the previous value of $0.42\ \delta_0$ where $\delta_0=0.76$ cm is the reference boundary-layer thickness at $x=45.2$ cm. In both cases, the relaxation parameters were $\lambda=6.7\ \delta_0$ and $s_0=45.2$ cm. The computed ramp pressure distributions were essentially identical, with no significant change in the extent of the interaction zone length. The principal effect of the finer streamwise mesh spacing was to move the separation point upstream by $0.2\ \delta_0$ and the reattachment point downstream by $0.02\ \delta_0$, and decrease the minimum skin friction coefficient from -0.69×10^{-3} to -0.88×10^{-3}. It should be noted that with $\Delta x=0.30\ \delta_0$, the separation region contained seven streamwise mesh stations. The sensitivity of the computation to the relaxation length was examined by recomputing region 2 using $\Delta x=0.30\ \delta_0$, $s_0=45.2$ cm, and $\lambda=13.4\ \delta_0$. The results were virtually identical to those for $\Delta x=0.30\ \delta_0$ and $\lambda=6.7\ \delta_0$. The separation point moved $0.006\ \delta_0$ downstream, with the minimum skin friction coefficient reduced to -0.93×10^{-3}. In summary, therefore, the mesh resolution is sufficient for accurate solution of the governing finite-difference equations, and the computed solution is relatively insensitive to the value of the relaxation length λ for the range $7\delta_0\lesssim\lambda\lesssim14\delta_0$ in essential agreement with previous studies.[22]

The absence of multiple spanwise measurements in the vicinity of the first ramp SBLI precludes a definitive judgment as to the possibility of significant three-dimensional flow in this region. Nevertheless, numerous experimental investigations[28,29] have demonstrated that shock-induced turbulent boundary-layer separation on a flat plate oftentimes exhibits a complex three-dimensional flow structure (a particularly striking example is shown in Fig. 16a in Ref. 29). The achievement of a nominally two-dimensional separated region (and hence a two-dimensional interaction zone) requires particular care due to the interaction of the incident and reflected shock with the sidewall boundary layers.[30-32] In the experimental study, the intent was to examine a simulated rectangular high-speed inlet for a variety of flight conditions and bleed schedules, and the existence of a significant three-dimensional flow structure in the neighborhood of separation is perhaps an accurate representation of the flow phenomena present in a prototype inlet design. In summary, therefore, it is the author's conjecture that the discrepancy in the extent of the computed and measured interaction zones is possibly attributable to significant three-dimensional flow structure in the region of flow separation.

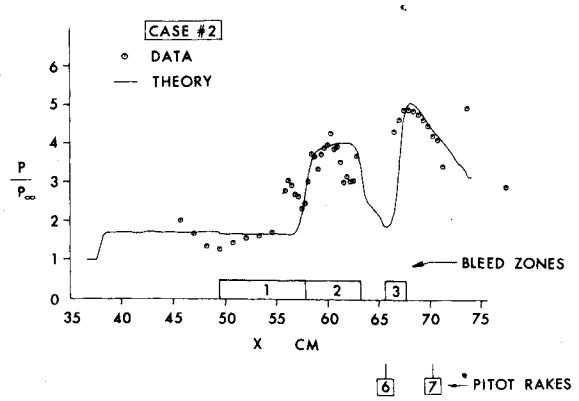

Fig. 9 Static pressure on cowl for case 2.

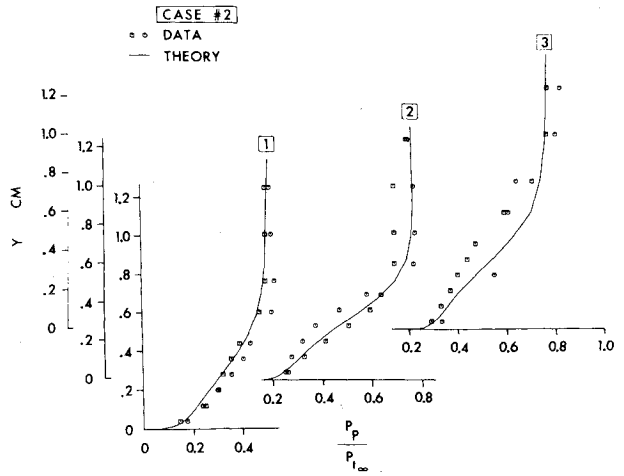

Fig. 10 Pitot pressure profiles on ramp at stations 1-3 for case 2.

The computed ramp pressure distribution in the vicinity of the second SBLI near $x=60$ cm is in reasonable agreement with experiment. The downstream displacement reflects the discrepancy in the origin of the interaction zone at the first SBLI as formerly discussed. The peak computed pressure is within 6% of the data.

The computed and measured cowl pressure is displayed in Fig. 9. The calculated pressure distribution is in good agreement with the data, and accurately predicts the peak pressures at the first and second SBLIs.

The ramp boundary-layer development is displayed in Figs. 10 and 11. The computed profile at station 1, located upstream of the first ramp SBLI, is in excellent agreement with the data. The profile at station 2, located downstream of the separation region, is similarly in very close agreement with the measurements. Comparison with the corresponding profile for case 1 (Fig. 5) clearly demonstrates the effect of boundary-layer bleed in the vicinity of the first ramp SBLI. The computed profile at station 3 is also in reasonable agreement with the data. In Fig. 11, the computed profile at station 4 is somewhat fuller than the experimental data, due possibly to the existence of significant three dimensionality in the flowfield near the second ramp SBLI as evidenced in the spanwise nonuniformity in the ramp static pressure at $x=66.0$ cm (see Fig. 8). The calculated profile at station 5 is in excellent agreement with the data.

The cowl boundary-layer development is shown on Fig. 12, where results are displayed at stations 6 and 7, located upstream and downstream of the second cowl SBLI. The calculated profile at station 6 is approximately 16% below the data, due possibly to the slight difference between the computed and experimental shock incidence locations at the second cowl SBLI (see Fig. 9). The computed profile at station 7 is in good agreement with the data.

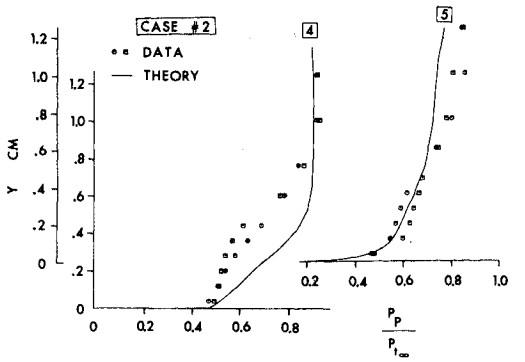

Fig. 11 Pitot pressure profiles on ramp at stations 4 and 5 for case 2.

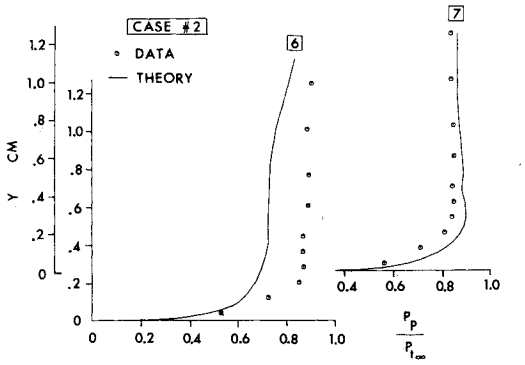

Fig. 12 Pitot pressure profiles on cowl at stations 6 and 7 for case 2.

Conclusions

An improved finite-difference code has been applied to the calculation of the flowfield in a simulated rectangular high-speed inlet. The algorithm is based on solving the full mean compressible Navier-Stokes equations in two dimensions with turbulence represented by an algebraic eddy viscosity. The method is capable of handling arbitrary inlet geometries through use of a numerical coordinate transformation. Provision is included for the specification of arbitrary boundary-layer bleed schedules on the ramp and cowl surfaces.

Calculations were performed for a simulated rectangular high-speed inlet at a Mach number of 2.5 and Reynolds number of 1.4×10^7 based on inlet length. Two different cases were considered, corresponding to "complete" and "partial" boundary-layer bleed schedules on the ramp. The computed ramp and cowl wall pressures and pitot pressure profiles were found in most instances to be in close agreement with the experimental data. In certain specific regions, agreement was limited due possibly to three-dimensional effects in the experimental flow and/or limitations of the turbulence model, although the qualitative features of the flowfield were nevertheless adequately represented.

Acknowledgments

Research sponsored by the Air Force Office of Scientific Research, Air Force Systems Command, USAF, under Grant AFOSR 80-0072, and the Air Force Flight Dynamics Laboratory, USAF, Wright-Patterson AFB, Ohio.

References

[1] Sorensen, V.L., "Computer Program for Calculating Flow Fields in Supersonic Inlets," NASA TN D-2897, 1965.

[2] Vadyak, J. and Hoffman, J., "Calculation of the Three-Dimensional Flow Field in Supersonic Inlets at Angle of Attack Using a Bicharacteristic Method with Discrete Shock Fitting," AIAA Paper 79-0379, Jan. 1979.

[3] Presley, L., "High Angle of Incidence Implications upon Air Intake Design and Location for Supersonic Cruise Aircraft and Highly Maneuverable Transonic Aircraft," NASA TM 78530, Sept. 1978.

[4]Sorensen, N., Smeltzer, D., and Latham, E., "Advanced Supersonic Inlet Technology," *Journal of Aircraft,* Vol. 10, May 1973, pp. 278-282.

[5]Reyhner, T. and Hickcox, T., "Combined Viscous-Inviscid Analysis of Supersonic Inlet Flowfields," *Journal of Aircraft,* Vol. 9, Aug. 1972, pp. 589-595.

[6]Gnos, A., Watson, E., Seebaugh, W., Sanator, R., and DeCarlo, J., "Investigation of Flow Fields within Large-Scale Hypersonic Inlet Models," NASA TN D-7150, 1973.

[7]Surber, L. and Sedlock, D., "Effects of Airframe-Inlet Integration on Half-Axisymmetric and Two-Dimensional Supersonic Inlet Performance," AIAA Paper 78-960, July 1978.

[8]MacCormack, R., "Numerical Solution of the Interaction of a Shock Wave with a Laminar Boundary Layer," *Lecture Notes in Physics,* Vol. 8, 1971, pp. 151-163.

[9]MacCormack, R. and Baldwin, B., "A Numerical Method for Solving the Navier-Stokes Equations with Application to Shock-Boundary Layer Interactions," AIAA Paper 75-1, Jan. 1975.

[10]Shang, J. and Hankey, W.L. Jr., "Numerical Solution for Supersonic Flow Over a Compression Ramp," *AIAA Journal,* Vol. 13, Oct. 1975, pp. 1368-1374.

[11]Deiwert, G.S., "Numerical Simulation of High Reynolds Number Transonic Flows," *AIAA Journal,* Vol. 13, Oct. 1975, pp. 1354-1359.

[12]Rakich, J., Vigneron, Y., and Tannehill, J., "Navier-Stokes Calculations for Laminar and Turbulent Hypersonic Flow Over Indented Nosetips," AIAA Paper 78-260, Jan. 1978.

[13]Shang, J., Smith, R., and Hankey, W.L. Jr., "Flow Oscillations of Spike-Tipped Bodies," AIAA Paper 80-0062, Jan. 1980.

[14]Knight, D., "Numerical Simulation of Realistic High Speed Inlets Using the Navier-Stokes Equations," *AIAA Journal,* Vol. 15, Nov. 1977, pp. 1583-1589.

[15]Knight, D., "Improved Numerical Simulation of High Speed Inlets Using the Navier-Stokes Equations," AIAA Paper 80-0383, Jan. 1980.

[16]Knight, D., "Calculation of High Speed Inlet Flows Using the Navier-Stokes Equations. Vol. I: Description of Results, Vol. II: User's and Programmer's Guide," AFFDL-TR-79-3138, Feb. 1980.

[17]Thompson, J., Thames, F., and Mastin, C., "Automatic Numerical Generation of Body-Fitted Curvilinear Coordinate System for Field Containing Any Number of Arbitrary Two-Dimensional Bodies," *Journal of Computational Physics,* Vol. 15, July 1974, pp. 299-319.

[18]Rubesin, M. and Rose, W., "The Turbulent Mean-Flow, Reynolds-Stress and Heat-Flux Equations in Mass-Averaged Dependent Variables," NASA TMX-62248, March 1973.

[19]Cebeci, T. and Smith, A.M.O., *Analysis of Turbulent Boundary Layers,* Academic Press, New York, 1974.

[20]Harris, J., "Numerical Solution of the Equations for Compressible Laminar, Transitional and Turbulent Boundary Layers and Comparison with Experimental Data," NASA TR T-368, 1971.

[21]Hopkins, E., Jillie, O., and Sorensen, V., "Charts for Estimating Boundary-Layer Transition on Flat Plates," NASA TN D-5846, June 1970.

[22]Shang, J., Hankey, W.L. Jr., and Law, C., "Numerical Simulation of Shock Wave-Turbulent Boundary Layer Interaction," *AIAA Journal,* Vol. 14, Oct. 1976, pp. 1451-1457.

[23]Keller, H., "Accurate Difference Methods for Nonlinear Two-Point Boundary Value Problems," *SIAM Journal of Numerical Analysis,* Vol. 11, April 1974, pp. 305-320.

[24]Carter, T. and Spong, E., "High Speed Inlet Investigation. Vol. I: Description of Program and Results. Vol. II: Data Summary," AFFDL-TR-77-105, Nov. 1977.

[25]Cebeci, T., "Variation of the Van Driest Damping Parameter with Mass Transfer," *AIAA Journal,* Vol. 11, Feb. 1973, pp. 237-239.

[26]Viegas, J. and Horstman, C., "Comparison of Multiequation Turbulence Models for Several Shock Boundary-Layer Interaction Flows," *AIAA Journal,* Vol. 17, Aug. 1979, pp. 811-820.

[27]Kuehn, D., "Experimental Investigation of the Pressure Rise Required for the Incipient Separation of Turbulent Boundary Layers in Two-Dimensional Supersonic Flow," NASA Memo 1-21-59A, 1959.

[28]Green, J., "Reflexion of an Oblique Shock Wave by a Turbulent Boundary Layer," *Journal of Fluid Mechanics,* Vol. 40, Jan. 1970, pp. 81-95.

[29]Green, J., "Interactions Between Shock Waves and Turbulent Boundary Layers," *Progress in Aerospace Sciences,* Vol. 11, 1970, Pergamon Press, pp. 235-340.

[30]Reda, D. and Murphy, J., "Shock Wave/Turbulent Boundary Layer Interactions in Rectangular Channels," *AIAA Journal,* Vol. 11, Feb. 1973, pp. 139-140.

[31]Reda, D. and Murphy, J., "Sidewall Boundary-Layer Influence on Shock Wave/Turbulent Boundary Layer Interactions," *AIAA Journal,* Vol. 11, Oct. 1973, pp. 1367-1368.

[32]Law, C.H., "Supersonic Shock Wave Turbulent Boundary Layer Interactions," *AIAA Journal,* Vol. 14, June 1976, pp. 730-734.